NUMERICAL COMPARISON OF THERMAL AND KINETIC MODIFICATION OF HYDROGEN AND OXYGEN

by

JOHN BENJAMIN GAITHER

A THESIS

Presented to the Faculty of the Graduate School of the

MISSOURI UNIVERSITY OF SCIENCE AND TECHNOLOGY

In Partial Fulfillment of the Requirements for the Degree

MASTER OF SCIENCE IN MECHANICAL ENGINEERING

2011

Approved by

Joshua L. Rovey, Advisor
David W. Riggins
Umit O. Koylu

ABSTRACT

This document describes a new modeling technique used to compare thermal and kinetic modification of hydrogen and oxygen gas. The thermal model uses an equilibrium thermodynamic analysis to determine the heat required for given mole fractions of molecular and dissociated products. A kinetic model is developed for a mono-energetic electron beam and a Maxwellian energy distribution. The kinetic model uses electron impact cross sections for excitation, dissociation, and ionization tabulated from available source data between 0-1000 eV. Cross sections are used to calculate forward reaction rates, electron penetration depths, and associated product concentrations for excited, dissociated, and ionized species. The preferred method of energy deposition must show faster rates of forward reaction and larger concentrations of products for lower energy requirements. Overall, thermal energy addition shows 50-90% dissociation in either gas but requires large amounts of energy (10^{7}-10^{8} kJ/kg). Kinetic modification, for the range of electron energies tested between 0-1000 eV, shows no significant change in the gas composition. Kinetically produced concentrations of excited, dissociated, and ionized molecules have orders of magnitude between 10^{-17}-10^{-14} mol/cm^{3} for the Maxwellian distribution and 10^{-19}-10^{-14} mol/cm^{3} for the mono-energetic beam. Qualitatively, the Maxwellian distribution provides faster rates of excitation, while the mono-energetic distribution provides faster rates of dissociation and ionization. Kinetic simulations apply less energy than the thermal model (i.e. 1000 eV = 1.602×10^{-16} J) and are one-dimensional in nature. Future simulations must include higher energies above 1000 eV, their associated cross sections, and Monte Carlo techniques to quantify the expected advantage of kinetic energy addition over thermal energy addition.

ACKNOWLEDGMENTS

I would like to thank my advisor for his efforts to guide and support me both academically and financially. I would also like to thank Dr. Umit Koylu and Dr. David Riggins for accepting positions as my committee members and offering advice and guidance on various aspects of this project. I also gratefully acknowledge the Department of Mechanical and Aerospace Engineering and the Missouri Space Grant Consortium for their financial support of my graduate studies. Without it, I would not have been able to pursue a graduate degree in a subject that I find immensely rewarding and enjoyable.

I also offer personal thanks to my family for their love, tireless support, and encouragement over the course of my undergraduate and graduate degrees. I thank them as well for the countless, immeasurable sacrifices they have made over the years to allow me to accomplish my dreams. I owe them a tremendous debt that I can never repay.

TABLE OF CONTENTS

LIST OF ILLUSTRATIONS

NOMENCLATURE

Symbol	Description
[A]	Molar concentration of dissociated atoms
$[A_2^*]$	Molar concentration of excited molecules
$[A_2]$	Molar concentration of molecules
$[A_2^{\pm}]$	Molar concentration of ions
[e-]	Electron concentration
[M]	Concentration of third body in chemical kinetic reaction
A	First stoichiometric reactant
a	Lower limit for rate coefficient integration
A_2	Diatomic molecule
A_2	Diatomic molecule
A_{2e}	Excited diatomic molecule
A_{2exit}	Molecule at exit plane
A_{2i}	Ionized diatomic molecule
A_{2inlet}	Inlet diatomic molecule
A_d	Dissociated atom
A_{exit}	Dissociated molecule at exit plane
B	Second stoichiometric reactant
b	Upper limit for rate coefficient integration
C	First stoichiometric product
d	Radius of sphere-of-influence
D	Second stoichiometric product
d_1	Hard sphere diameter of electron
d_2	Hard sphere diameter of molecule
dS	Differential area
dV	Differential volume
e	Internal energy
E_{el}	Electron energy
E_{new}	Electron energy at new iteration step

E_{old}	Electron energy at previous iteration step
f(E)	Energy distribution function
f_b	Body force
g	Gravitational constant
h_f^o	Enthalpy of formation
h_p	Enthalpy of product species
h_r	Enthalpy of reactant species
h_t	Total enthalpy
k	Boltzmann constant
k_a	Absorption rate coefficient
k_d	Dissociation rate coefficient
k_e	Excitation rate coefficient
k_f	Forward rate coefficient
k_i	Ionization rate coefficient
K_p	Equilibrium constant
k_{rc}	Recombination rate coefficient
m	Gas mass
$\dot{m}$	Mass flow rate
M	Third body in chemical kinetic reaction
m_{el}	Electron mass
n	Gas number density
$\dot{n}$	Molar flow rate
n	Normal vector to surface element dS
N	Number of particles
N_m	Number of moles
N_p	Number of moles of products
N_r	Number of moles of reactants
P	Pressure
P_1	Inlet pressure
P_2	Exit pressure
Q	Thermal energy input

$\dot{Q}$	Heat transfer rate
R_u	Universal gas constant
T	Temperature
t	Time in seconds
T_1	Inlet temperature
T_2	Exit temperature
T_{el}	Electron temperature
T_p	Product temperature
T_r	Reactant temperature
V	Cylinder volume
v	Electron velocity
v_{th}	Thermal velocity
X	Mole fraction
X_A	Mole fraction of species A
x_d	Penetration depth
y_e	Exit height
y_i	Inlet height
α	Mass fraction
Δh	Difference between enthalpies at specified state and reference state
λ	Mean free path
ν_A	Stoichiometric coefficient for product A
ν_B	Stoichiometric coefficient for product B
ν_C	Stoichiometric coefficient for product C
ν_D	Stoichiometric coefficient for product D
ν_{H2p}	Stoichiometric coefficient for molecular hydrogen product
ν_{Hp}	Stoichiometric coefficient for dissociated hydrogen product
ρ	Fluid density
σ	Energy dependent cross section
τ	Shear force

1. INTRODUCTION

1.1. LITERATURE REVIEW

Control of combustion processes can be accomplished through thermal or kinetic modification of constituent gases involved in combustion cycles. Such control mechanisms can modify many different aspects including ignition temperatures, ignition delay times, flame temperatures, or, in the case of this research, mole fractions and concentrations of final products and free radicals involved in combustion. Active modification allows tailoring of the process to expand the optimal range over which a combustion process operates. Kinetic modification promises the ability to affect specific species in reactions and may allow better performance in fuel rich and fuel lean operation.

Thermal modification is heating of the gas to raise its temperature. The temperature rise allows various molecules and atoms in the gas to undergo processes such as excitation, dissociation, or ionization, and various chemical reactions depending on the amount of thermal energy input into the system and the initial thermodynamic state of the gas. These chemical changes, however, occur over all species in the gas, regardless if a change in a single species is desired. As a result, thermal methods also require large amounts of power (~*kW*) for flow rates on the order of grams per second. For these reasons, unless power requirements can be reduced, thermal modification is currently not a feasible method for improving combustion performance.

Kinetic modification can be performed by applying a beam of electrons with a specific energy distribution to a gas in order to cause an increase in energy (temperature) of a specific species of that gas. Kinetic modification targets specific reactions. This type of modification is related to the different electron-impact cross sections found at various electron energies for specific elements and molecules. These cross sections imply a probability of being able to target a specific species to cause changes in the chemical composition of the gas. A larger cross section means a greater chance for a given reaction to occur. Depending on the energy of the electrons (and hence the cross section size), a given electron impact can generate excited atoms or molecules, dissociated molecules, or ions of a specific species in the bulk volume of the parent gas.

A kinetic process, then, can allow for the breakup of specific components of gaseous mixtures while leaving the remaining gaseous species largely unaffected. Kinetic processes can be used to tailor combustion processes to produce more free radicals of a specific type during combustion thereby modifying the global and sub-reactions and the products they create.

The advantages and disadvantages of plasma-assisted combustion (PAC) are intensely studied topics. There has been a large amount of experiments in PAC in recent years. Such experiments are good for providing insight into the results of applying plasma discharges to modify flame properties and other aspects of combustion processes. However, these experiments lack some ability in elucidating a more intimate, fundamental understanding of why particular results occur. Plasma-assisted combustion (PAC) processes were reviewed by Starikovskaia [1]. She found, among other items, that a gas can be modified by non-equilibrium plasma. In such a process, the gas is modified by impact with electrons produced through a typical discharge. For reduced electric field values between "100 - 300 Td", reaction rates were seen to be between "$10^{-10} – 10^{-8}$ cm^3/s" which was approximately 2 orders of magnitude higher than the thermal reaction rate [1]. PAC can be accomplished through the use of various discharges such as atmospheric pressure glow discharge (APGD), dielectric barrier discharge (DBD), streamer discharge, and pulsed nanosecond discharges [1]. APGD is a general name for discharges which can generate non-equilibrium plasma at atmospheric pressure [1]. A DBD is formed for a discharge occurring when at least one electrode is covered by dielectric [1]. They have been used in past years for ozone generation. "Densities of dissociated and excited species are within the range $10^{12} – 10^{14}$ cm^{-3} [1]." A streamer discharge "is a non-equilibrium low temperature plasma with relatively high electric fields in the streamer's head and low fields in the channel [1]." The author observed from Pancheshnyi and Starikovskaya, that for a streamer diameter of 1 mm, excited nitrogen densities were approximately 10^{-12} cm^{-3} [1]. Pulsed nanosecond discharges are of interest in combustion processes since they develop on much smaller time scales than those required for ignition and can produce a spatially uniform plasma [1]. Using plasmas to augment combustion processes has been a subject of great study. Some of this research has been conducted on "breakdown ignition systems for use in internal combustion

engines to initiate combustion [1]. Plasma can also be used to modify flame fronts and allow engines to operate in fuel lean conditions [1]. Plasma ignition has further applications in aerospace propulsion with reducing ignition delay times and enhancing low pressure flame holding. These concepts rely on microwave (MW) and RF discharges [1]. Different experiments provide mixed results. Experiments in the ignition of propane-air mixtures have shown both that a discharge with a higher degree of reduced electric field give shorter induction times, and also that there may be cause to say that any type of excitation that occurs is good, as long as it increases the rate of reaction [1]. Plasma can further be used in combustion sustainment in low speed flows. In this application, plasma discharges can be used to modify flame blow-off velocities in premixed flames. These discharges can also be used in jet diffusion flames to control flame liftoff from a burner. Discharges such as DBD and pulsed nanosecond discharge increased flame stability limits were capable of causing liftoff itself or reattaching the flame [1]. In general, a more understanding of the interplay between chemical kinetics, discharge physics, and hydrodynamics in PAC is highly desired.

In general, experiments have used electron beams or electric discharges which produce either thermal or non-thermal plasmas. Thermal plasma generation results in heat addition to all fluid components over all degrees of freedom [2]. This results in large gas temperatures above 5000 K and does not easily allow selection of specific chemical reactions [2]. Non-equilibrium plasma discharges, such as the gliding arc discharge used by Ombrello's group, produce more focused selectivity for chemical reactions [2]. Their particular version used up to 286 W of power with current densities between 5-55 A/cm^2 [3]. Average electron energies in their experiment ranged between 1.1 eV and 4.75 eV. Results showed that there were large amounts of free radicals produced but these amounts were hindered by large recombination rates. . They found that larger power levels were required to achieve higher gas temperatures unless the gas was preheated to a few hundred Kelvin below ignition or extra fuel was injected just upstream of the plasma location [3]. Results exhibited an increase in concentrations between 2-7 ppm at 300 K to between 41-71 ppm at 1200 K. The existence time of free radicals was also found to increase by decreasing the pressure from 1 atm to 0.1 atm [3]. Electron beams can also be used to alter flows entering scramjet engines. One concept

suggested that an electron beam be used for ion generation in a “hypersonic cold-air” MHD device used to generate power or accelerate flows in a scramjet models developed in AJAX and MARIAH II [4]. A non-thermal, high energy electron beam (~keV) is needed since such MHD devices operate with flow at the inlet in tenths of atmospheres and hundreds of Kelvin, making traditional thermal ionization methods impractical [4]. Since cross section size increases for decrease in electron energy, electron beams showed promise for causing ionization in the interior of the MHD channel, away from hot boundary layers [4].

Kinetic modification can also be beneficial in altering harmful compounds that result from combustion processes. Electric discharges and electron beams can be shown to be useful in the breakup of NO_x and volatile-organic-compounds (VOCs) [5]. For instance; reduction of NO is accomplished by use of an electron beam. In such a case, the electron beam was shown to produce concentrations up to a factor of 6 greater than a pulsed corona discharge for energy densities up to 20 J/L. The electric discharge was shown to require energy densities up to 120 J/L [4]. For VOC’s such as CCl4, the electron beam was found to be around a factor of 60 less than the pulsed corona discharge. For reduction of CCl4, the electron beam energy density was again around 20 J/L while the pulsed corona discharge required approximately 1270 J/L [5]. Kinetic modification is analyzed for two different cases. These cases are a mono-energetic and a Maxwellian energy distribution. A mono-energetic beam can be produced by an electron gun which emits electrons at a specific energy. Electron guns can be found in various aspects of life from everyday items such as televisions which use cathode-ray tubes to electron microscopes. It generally consists of a cathode which emits the electrons and an electromagnetic or electrostatic device which focuses the beam to a specific energy. A Maxwellian energy distribution can be produced by electric discharges such as gliding arc, pulsed corona, or dielectric barrier discharges used in plasma generation. Figure 1.1 provides diagrams of devices used to produce each type of energy distribution [5].

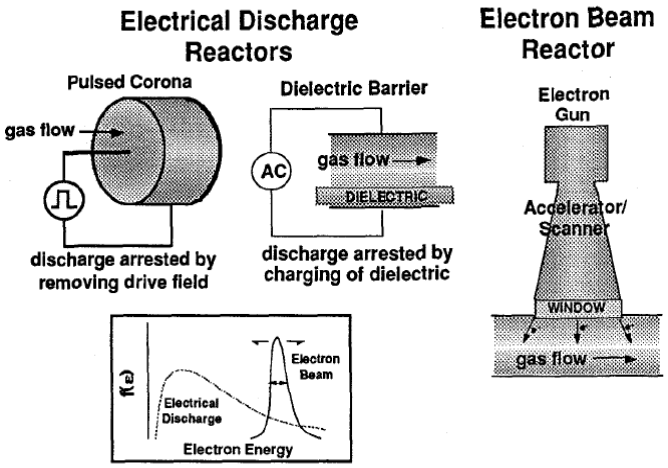

Figure 1.1. Devices to produce energy distributions [5]

1.2. RESEARCH OBJECTIVES

There are two sets of objectives for this project. The first objective of this research is to obtain a fundamental understanding of kinetic energy addition processes, electron impact cross sections, and gas kinetic theory. The second objective is to compare results of thermal and kinetic modification of a gas by numerical analysis. Thermal energy addition data will be compiled for uniform heating of H_2 and O_2. Kinetic energy addition data will be compiled for 2 energy distribution functions applied to H_2 and O_2: a mono-energetic electron beam and a Maxwellian distribution. Data to be calculated include reaction rates, concentrations, and mole fractions. Analysis of supplied data should determine which of the aforementioned modes of energy addition supply the best, most desired results in terms of products and concentrations produced. Models and their corresponding data were generated by Matlab codes contained in an appendix on CD-ROM. This appendix is available upon request from the Office of Graduate Studies or Curtis Laws Wilson Library at the Missouri University of Science and Technology.

2. THERMAL MODEL

2.1. THERMAL MODEL GEOMETRY

The thermal model assumes a cylinder into which either molecular hydrogen (H_2) or molecular oxygen (O_2) is introduced at a given mass flow rate, temperature, and pressure. This modeling technique is intended to be used with any analysis involving chemical reactions or combustion processes involving low speed flows. Therefore, changes in kinetic energy (large velocity change) are neglected in this analysis. Flows for supersonic or hypersonic combustion are specifically excluded, since such flows would involve very large kinetic energy changes between the flow through the device and ambient surroundings. Flow rates are assumed to be constant for the thermal model, and the flow is assumed to move only in the positive x-direction. Frictional effects are also ignored in this problem. Inlet temperature T_1 is 300 K. Pressure is held constant for this problem. Molar ratios of H to H_2 or O to O_2 at the exit plane are chosen between 1:20 and 2:1. Mass flow rate was 10 g/s. The required amount of heat transferred Q and the exit temperature are the quantities to be obtained. Thermal energy Q, in the form of heat, is added uniformly at a constant rate. Products of reaction are assumed to be in chemical equilibrium at the exit. A diagram of the problem is shown in Figure 2.1. In Figure 2.1, the heat transfer over the length and circumference is represented by Q and the dashed, vertical arrows. The variable A_{2inlet} and A_{2exit} represent reactant or product molecules at the inlet and exit, respectively. The variable A_{exit} represents the dissociated A_{2exit} molecules present at the exit. Thermal ionization processes are not considered. Note that the use of a cylinder is completely arbitrary. The volume can have a cross section of any geometrical shape.

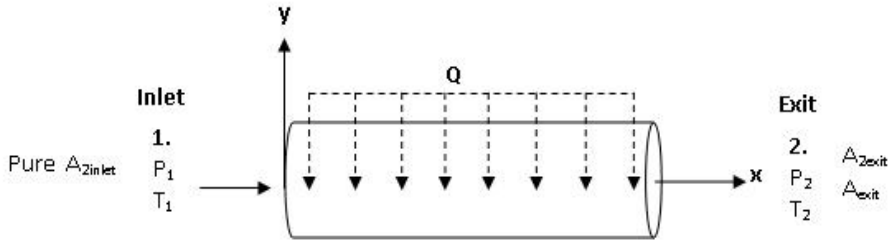

Figure 2.1. Thermal model geometry

2.2. THERMAL MODEL THEORY

Stoichiometrically, the thermal model is based on the simple dissociation reaction where either H_2 breaks down into 2H or O_2 breaks down into 2O. These cases are represented by Eq. 1 and Eq. 2.

$$H_2 \leftrightarrow 2H \tag{1}$$

$$O_2 \leftrightarrow 2O \tag{2}$$

The above equations assume that the reactant molecule undergoes only dissociation. Equation 1 and Eq. 2 do not account for ionization of species. In reality, the actual products produced by dissociation reactions are more closely modeled according to the global, overall reaction shown in Eq. 3.

$$\nu_A A + \nu_B B \rightarrow \nu_C C + \nu_D D \tag{3}$$

In Eq. 3, *A* and *B* represent the reactant molecules (H_2 or O_2) and ν_A and ν_B represent the number of moles of reactant *A* and *B*. The variables *C* and *D* represent the products formed, which are H_2 and H or O_2 and O. The variables ν_A, ν_B, ν_C, and ν_D are stoichiometric coefficients which represent the molar amounts of reactants or product that are formed as a result of reaction. Equation 3 implies that a direct conversion of all

molecular reactants to all dissociated products does not necessarily take place. A more effective process will result in a larger mole fraction of dissociated molecules and fewer unaltered molecules. It should be noted that Eq.1 and Eq. 2 indicate an equilibrium state, where reactants and products exist simultaneously.

To describe mole fractions, only the forward portion of Eq. 1 and Eq. 2 were considered. In this case a hydrogen or oxygen molecule dissociates into its two, constituent atoms (H or O). Exit mole fractions are represented by *X*, where a specific species mole fraction is represented by an appropriate atomic symbol as a subscript. They are obtained by applying the stoichiometric ratio of dissociated atoms to unaffected molecules at the exit. For example, if the ratio was 1 mole of H for every 5 moles of H_2, then the total moles at the exit is 6, and the mole fraction for H_2 is 5/6 or approximately 0.83. The mole fraction for H is then 1/6 or approximately 0.16. Product mole fractions can then be used along with their partial pressures to determine the value of the equilibrium constant K_p. Equation 4 provides an example of the equation for mole fractions using the fraction of H formed from H_2. Similar equations exist for other products.

$$X_H = \frac{x_H}{x_H + x_{H_2}} \tag{4}$$

The equilibrium constant K_p is a measure of how likely a reaction is to occur and go to completion favoring products. A K_p value much greater than 1 indicates that the reactions goes strongly to completion and favors the products. Values much less than 1 indicate that the reaction is unlikely to occur. Equilibrium constants are represented in terms of the partial pressures of products over the partial pressures of reactants and the stoichiometric coefficients from Eq. 3. The required relationship is shown in Eq. 5.

$$K_p = \prod_{i=1}^{N} P_i^{\nu_i'' - \nu_i'} = P_A^{2-0} \cdot P_{A_2}^{0-1} \tag{5}$$

In Eq. 5, P_i is the partial pressure of the i^{th} reactant and N is the total number of products present. The stoichiometric coefficients for products are denoted by ν_i'', and

stoichiometric coefficients for reactants are represented by v_i'. On the right side of the equation, P_A and P_{A2} refer to the partial pressures of dissociated atoms and molecules present after reaction. Partial pressures of reactants and products can be determined from mole fractions and Dalton's Law of Partial Pressures which states that the total pressure is the sum of the individual pressures of each component of a gas. Partial pressures are the mole fraction of a particular gas species multiplied by the total pressure P of the gas. The equilibrium constant can be represented in terms of stoichiometric coefficients and partial pressures as shown in Eq. 6. In Equation 6, *p* and *i* subscripts refer respectively to products and reactants. Total pressure of the gaseous mixture is represented by P. Mole fractions of dissociated atoms are denoted by X_A, and mole fractions of molecules are denoted by X_{A2}. Stoichiometric coefficients for dissociated atoms are ν_{Ap}. Stoichiometric coefficients for molecules are $\nu_{A2.}$

$$K_p = \frac{(X_A P)^{\nu_{Ap} - \nu_{Ai}}}{(X_{A_2} P)^{\nu_{A2p} - \nu_{A2i}}} \tag{6}$$

Exit temperatures for products can be found by taking the natural logarithm of K_p and applying this value to JANNAF Thermochemical Tables [6]. These tables are temperature based, and interpolation can be used to find exit temperatures for natural logarithm of K_p values that fall between known data points in the tables. Once the exit temperature is known, a standard energy balance based on a chemically reacting system can be used to find the amount of thermal energy addition required to raise the temperature from T_1 at the tube entrance to T_2 at the tube exit.

The appropriate energy balance states that the change in the energy of the system is equal to the sum of the change in energy of a state and the change in energy due to changes in chemical composition. If both reactants and products are in a gaseous state, then the energy change of the system is due only to the chemical reactions taking place inside the tube due to thermal heat addition [7]. The amount of energy input must equal the amount of energy output. For a reacting system, the energy balance includes contributions of heat and work. The contribution of these quantities is shown in Eq. 7.

$$\frac{\partial}{\partial t}\iiint_V \rho\left(e+\frac{\vec{V}\cdot\vec{V}}{2}\right)dV + \iint_S \rho h_t(\vec{V}\cdot\hat{n})dS =$$

$$\iint_S (\vec{\tau_S}\cdot\vec{V})dS + \iiint_V \rho\vec{f_b}\,\vec{V}dV + \dot{Q}_{tot} + \dot{W}_{shaft} \qquad (7)$$

The first term on the left side is a time rate of change, which is zero for a steady flow assumption. The work rate of the body force is also neglected. Since there are no shafts crossing the boundaries of the control volume, the shaft work term is also neglected. Viscous effects are also neglected. The energy flow rate term on the left is a function of total enthalpy h_t (per mass) which is described in Eq. 8 as the sum of the internal and kinetic energies.

$$h_t = \left(e+\frac{p}{\rho}\right)+\left(\frac{\vec{V}+\vec{V}}{2}\right) \qquad (8)$$

Using the stated assumptions, Eq. 7 can be rewritten as Eq. 9.

$$\iint_S \rho h_t(\vec{V}\cdot\hat{n})dS = \dot{Q}_{tot} \qquad (9)$$

Equation 9 states that the total rate of heat transfer is equivalent to the net enthalpy flow rate out of the control volume. If low flow velocity is assumed, the change in the kinetic contribution to total energy can be ignored. The rate of heat transfer can be represented as the net change in enthalpy between the products and reactants as shown in Eq.10. Since there are multiple reactant and product species, the enthalpy for each of these components must be accounted for by the mass fraction α. The mass fraction α is the percentage amount (by mass) of a given species found in the gaseous mixture. Note in Eq. 10 that g is the gravitational constant, and y is the height of the inlet or exit of the duct.

$$\dot{Q}_{tot} = \Sigma_{prod}\dot{m}[\alpha h_p + g y_e] - \Sigma_{react}\dot{m}[\alpha h_r + g y_i] \qquad (10)$$

Neglecting potential energy changes for reactants and products gives the energy equation as shown in Eq. 11.

$$\dot{Q}_{tot} = \sum_{prod} \dot{m}(\alpha h_p) - \sum_{react} \dot{m}(\alpha h_r) \tag{11}$$

Dividing by the molecular weight (in appropriate units) will give Eq. 11 on a molar basis where the mass flow rate will become the molar flow rate. Molar flow rates at the inlet will then be those associated with reactants, and molar rates at the exit will be associated with products. Exit enthalpy will be associated with products and inlet enthalpy will be associated with reactants. Enthalpies for products and reactants can be described as the sum between the enthalpy of formation and the sensible enthalpy. Combining these statements and assumptions for the first law as applied to a reacting, steady flow produces Eq. 12.

$$\dot{Q}_{tot} = \sum_{prod} \dot{n}(\overline{h_f^o} + \Delta\bar{h}) - \sum_{react} \dot{n}(\overline{h_f^o} + \Delta\bar{h}) \tag{12}$$

Equation 12 states that the heat transfer is equivalent to the difference between the enthalpy of products and the enthalpy of reactants. In Eq. 12, the term in parentheses within each summation is the enthalpy on a molar basis at a specified temperature of reactants T_r or product temperature T_p. The Δh term is the difference between standard enthalpies at the specified and reference states (sensible enthalpy) [7]. Heats of formation of reactants and products are represented by h_f^o. Heats of formation of naturally occurring, stable elements such as O_2 and H_2 are zero at 298 K and 1 atm. Rearranging Eq. 12 and dividing by molar flow rates of fuel allows a solution for the heat addition in terms of molar amounts of reactants and products. This produces Eq. 13 where N_{mr} and N_{mp} are the number of moles of reactants or products (per mole of fuel), respectively.

$$Q = \sum_{prod} N_{mp}(\overline{h_f^o} + \Delta\bar{h})_{Tp} - \sum_{react} N_{mr}(\overline{h_f^o} + \Delta\bar{h})_{Tr} \tag{13}$$

Equation 13 is used in the numerical analysis to calculate the energy necessary for specified exit mole fractions. Values for N_{mp} and N_{mr} in one second can be found by multiplying the known mass flow rate by the time *t* and dividing this result by the molecular weight of the reactant or product gas species. Heat of formation data are obtained by using published tables such as Table A.3, A.4, A.11, and A.12 in Appendix A of An Introduction to Combustion, Concepts and Applications 2ed by Stephen R. Turns [8]. These tables used in this text were generated from "The Chemkin Thermodynamic Database," Sandia Report, SAND87-8215B, March 1991. Interpolation is used when data falls between listed points in the tables. Molar concentrations of products can be obtained from a modification of the gas equation-of-state given in Eq. 14. Note if change in kinetic energy was included, a coupled system of equations (momentum, energy, continuity, and equation-of-state would have to be solved simultaneously for exit temperature, exit pressure, and exit velocity.

$$[A] = \mathrm{X}_A \frac{P}{R_u T} \tag{14}$$

In Eq. 14, X_A represents the mole fraction of species *A*. Mixture pressure (sum of all partial pressures) is represented by *P*, and the universal gas constant (8314 J/kgK) is represented by R_u. The variable *T* is the temperature. Molar amounts of reactants can be found by multiplying the known mass flow rate by the operation time *t* in seconds and dividing this value by the molecular weight of the gas. Molar amounts of products can be found by conducting an atom balance using Eq. 3 for one second. For instance, if the ratio of dissociated H (product) to H_2 reactant was 1/5, then the following equations allow determination of molar amounts of products produced by the dissociation reaction.

$$2\nu_{H_2} H_2 \rightarrow 2\nu_{H_2} H_2 + \nu_H H \tag{15}$$

$$\frac{\nu_{H_p}}{\nu_{H_{2p}}} = \frac{1}{5} \tag{16}$$

$$2\nu_{H_2} H_2 \rightarrow \nu_{H_{2p}} H_2 + \frac{1}{5}\nu_{H_{2p}} H \tag{17}$$

Solution of Eq. 17 provides v_{H2p} and allows determination of v_{Hp} in Eq. 16 from a given number of moles. In Eqs. 15-17, the stoichiometric ratio of dissociated atoms to unaltered molecules is varied in the numerical simulation. Similar equations and a corresponding solution exist for oxygen dissociation.

3. KINETIC MODEL

3.1. KINETIC MODEL GEOMETRY

Kinetic modification of a gas is assumed to occur by impacting a target molecule (or molecules) with a beam of electrons. The impact of the electron on the molecule causes excitation, dissociation, or ionization of that molecule. Which inelastic collision that occurs depends on the energy of the electron and the impact cross section associated with that energy. The kinetic model uses geometry similar to the thermal model described in Section II to solve for the exit concentrations of excited, dissociated, or ionized molecules or atoms. However, the application of uniform heat at a constant rate is replaced by the application of an electron beam at the origin (0, 0, 0) with either a mono-energetic or Maxwellian energy distribution. The kinetic geometry is shown in Figure 3.1. In Figure 3.1, e- represents the application of electrons to the gas from a point source at the origin. At the exit, A_2 denotes unaffected molecules, A_{2e} denotes excited molecules, A_d represents dissociated atoms, and A_{2i} represents ionized molecules. The source is either an electric discharge gun or an electron beam that produces energies between 0 eV and 1000 eV. Electron energy is assumed to be only kinetic energy. Electrons in the beam move only in the positive x-direction (+ to the right in Figure 3.1). Scattering effects on the electrons are ignored.

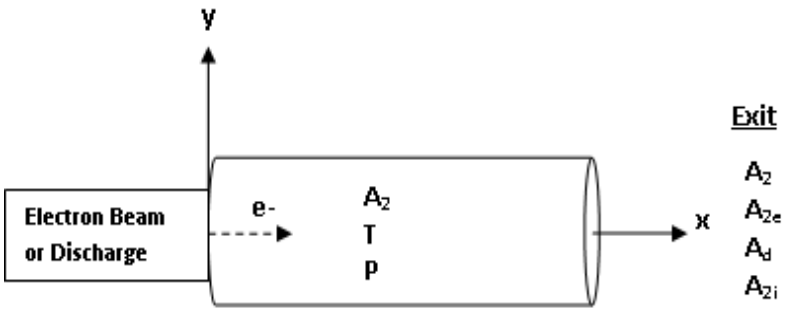

Figure 3.1. Kinetic model geometry

3.2. GAS KINETIC THEORY

This particular model calculates the molar amounts, concentration rates, concentrations, and rate coefficients for excitation, dissociation, and ionization reactions in a single gas. These quantities are functions of the energy-dependent electron impact cross sections. Calculation of the needed quantities first requires determination of the kinetic, forward rate coefficients for a given type of energy distribution.

3.2.1. Rate Coefficients. The rate coefficient k_f is defined as the rate of change of a given species concentration (i.e. how fast reactants are converted to products). To obtain the temperature-dependent rate coefficient, the rate coefficient for a well-defined, relative velocity must be integrated over a given energy distribution *f(E)* [9]. This thermal averaging is described by Eq. 18 [9].

$$k_f(T) = \int_a^b f(E)\sigma(E)v(E)dE \tag{18}$$

Within Eq. 18, the energy distribution function is represented by *f(E)*, and the collision cross section is *σ(E)*. The velocity term *v* is the electron velocity in m/s. Integration is carried out between 0 and infinity. Electron velocity can be obtained from its kinetic energy. Assuming one-dimensional motion for the electron, then, results in Eq. 19 for the kinetic energy (KE) where m_{el} is the mass of the electron.

$$KE = E_{el} = \frac{1}{2}m_{el}v^2 \tag{19}$$

Equation 19 can be rearranged to solve for the electron velocity. Electron velocity is then provided as a function of known electron energy (eV) in Eq. 20.

$$v = \sqrt{\frac{2E_{el}}{m_{el}}} \tag{20}$$

The energy distribution function *f(E)* must also be defined. As stated, there are two energy distributions considered for the kinetic model: a mono-energetic electron beam

and a Maxwellian energy distribution. A conceptual diagram of the two distributions is shown in Figure 3.2. In Figure 3.2, *f(E)* is the energy-distribution function, E_{el} represents the electron energy, $f_{maxwell}$ labels the Maxwellian distribution curves (solid and dashed lines), and f_{mono} labels the mono-energetic distribution (solid vertical line).

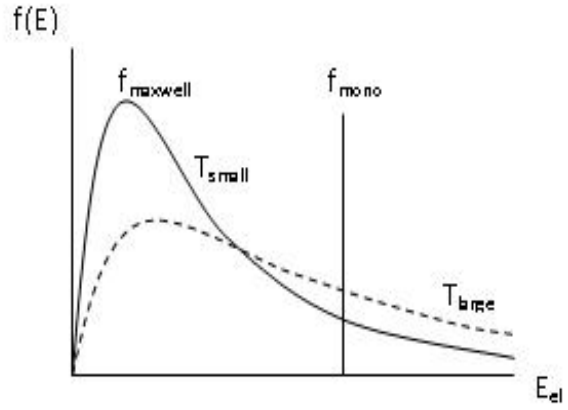

Figure 3.2. Conceptual diagram of energy distributions

As shown in Figure 3.2, electrons in a Maxwellian distribution are distributed over a wide range of energies, with a larger number of electrons populating lower energies compared to higher energies. The solid curve labeled with T_{small} represents low electron temperature and the dashed curve labeled with T_{large} represents higher electron temperatures. The peak on the Maxwellian curve becomes shallower and the curve broadens as the electron temperature T_{el} is increased. This allows more electrons to populate higher energies. The mono-energetic beam contains electrons which are all at the same energy. The Maxwellian energy distribution is an isotropic distribution that can be described by Eq. 21 [10].

$$f(v) = 4\pi n\left(\frac{m}{2\pi kT}\right)^{3/2} v^2 exp\left(\frac{-v^2}{v_{th}^2}\right) \tag{21}$$

In Eq. 21, v is the electron velocity (based on kinetic energy) and v_{th} is the thermal velocity, k is the Boltzmann constant, n is number density, m is gas mass, and T is temperature. Realizing that v^2 can be represented in terms of the kinetic energy and mass, Eq. 22a and Eq. 22b can be obtained.

$$v^2 = \frac{2E_{el}}{m} \tag{22a}$$

$$f(v) = 4\pi n\left(\frac{m}{2\pi kT}\right)^{3/2}\left(\frac{2E_{el}}{m}\right)\ exp\left(\frac{-v^2}{v_{th}^2}\right) \tag{22b}$$

Once again, k is the Boltzmann constant, n is number density, m is gas mass, T is temperature, v is the electron velocity, and v_{th} is the thermal velocity. Rearranging the $2E_{el}/m$ term in Eq. 22b produces Eq. 23.

$$f(v) = \frac{\sqrt{2}}{\sqrt{\pi}}\left(\frac{2\sqrt{\frac{m}{kT}}E_{el}}{kT}\right)exp\left(\frac{-v^2}{v_{th}^2}\right) \tag{23}$$

Simplifying Eq. 23 produces Eq. 24.

$$f(v) = \frac{2}{\sqrt{\pi}}\sqrt{2mn}\left(\frac{1}{kT}\right)^{3/2}(E_{el})exp\left(\frac{-v^2}{v_{th}^2}\right) \tag{24}$$

Inserting Eq. 22a into the numerator of the exponential term in Eq. 23 and simplifying creates Eq. 25.

$$f(E) = \frac{2}{\sqrt{\pi}}\left(\frac{1}{T_{el}}\right)^{3/2}\sqrt{E_{el}}exp\left(\frac{-E_{el}}{T_{el}}\right) \tag{25}$$

Equation 25 is the Maxwellian distribution function used in this analysis. The electron temperature variable is represented by T_{el} and electron energy range for the distribution is

represented by E_{el}. Note, as stated previously, increasing the electron temperature will decrease the maximum value of *f(E)*, and decreasing T_{el} will increase the maximum value. The mono-energetic function value is set to 1.0 in the model since all electrons are at the same energy. Integration of this distribution produces a single function value for a given energy.

Once the distribution functions, cross sections, and electron velocity have been determined, the forward rate coefficient k_f for excitation, dissociation, and ionization can be calculated by Eq. 18. Limits on the range of cross section data (0 eV and 1000 eV) correspond respectively to the integration limits *a* and *b* found in Eq. 18.

3.2.2. Cross Sections. A collision can result in anything from chemical reactions or a perturbance from the original direction of motion. For the analysis of this problem, a collision is assumed to cause a chemical change in the system. These collisions and the associated reactions they cause are governed by the electron impact energy and the energy dependent cross section. Cross sections used in the kinetic model are obtained from tabulated source data. This tabulated data was placed into a cross section database in Matlab for use in the calculation of the rate coefficient integrals for each energy distribution. References 11 and 12 were used for construction of the hydrogen and oxygen databases. Cross sections in the electron energy range between 0 eV and 1000 eV were taken for excitation, dissociation, and ionization from each respective source. Note that cross sections were only presented in the oxygen source up to 998 eV. Cross sections are an input for calculation of the rate coefficients. There is some error associated with each cross section data set. Excitation data for hydrogen contains an error range of ±20 percent, and hydrogen dissociation error is ±20 percent [11]. Hydrogen ionization error is within ±5 to ±7 percent [11]. For oxygen excitation, error is within 20 percent while oxygen dissociation error is ±34 percent [12]. Oxygen ionization error is ±5 percent [12]. Tabulated cross sections are plotted in Figure 3.3.

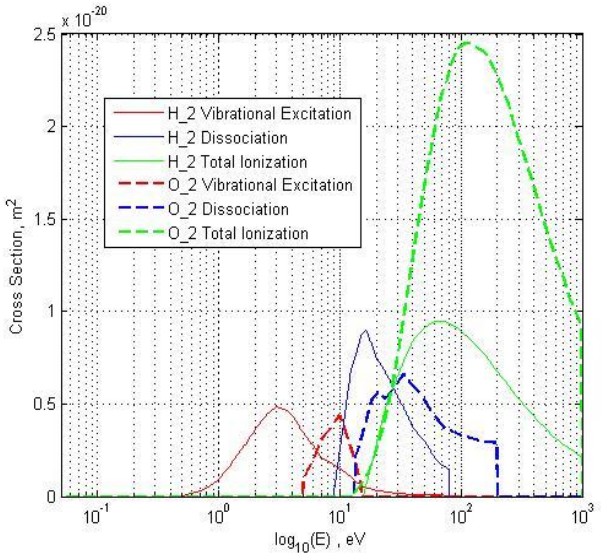

Figure 3.3. Electron impact cross sections for H_2 and O_2 plotted from source data [11], [12]

Fundamentally, the cross section term $\sigma(E)$ in Eq. 18 is the size of the target the electron has to hit in order for a collision and a reaction to occur. The size of the cross section is dependent on the electron energy. More specifically, a cross section can be described using the assumption of a hard sphere model. This method assumes that the electron and the molecule have hard sphere diameters d_1 and d_2 respectively, of finite size, much like billiard balls. A sphere of influence with a radius d equal to the sum of the radii of each particle can be used to describe the effective range of the intermolecular forces [9]. Figure 3.4 describes the hard sphere collision. In this figure, the electron is represented by the smaller circle of radius d_1. The molecule is represented by the larger circle of radius d_2. The x and y axes are in the plane of the paper, while the z-axis points out of the page.

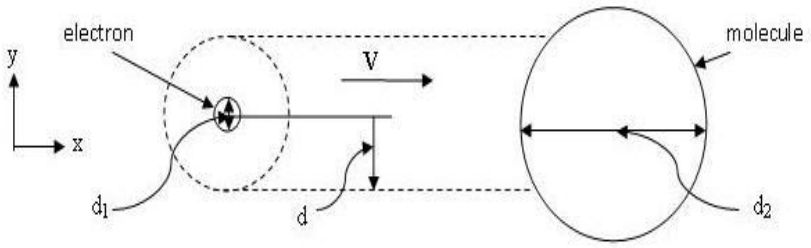

Figure 3.4. Hard sphere collision

For Figure 3.4, consider a beam electron moving in a straight line with a velocity *v* through a target gas. As the electron moves through the gas, it sweeps out a cylindrical volume equal to $\pi d^2 x$. In this volume, the *d* term represents the radius of the sphere-of-influence associated with the circular cross section πd^2 perpendicular to the velocity vector. This value of *d* is related to the effective range of intermolecular forces and is energy dependent [9]. A collision occurs when the center of one particle lies on or within the "sphere of influence" of the other particle [9]. In other words, the "cross section is that area […] that the relative motion of the molecules needs to cross if a collision is to take place [9]."

The model builds the cross section database by expanding the number of energy and cross section points by linear interpolation over the relevant energy ranges. The use of linear interpolation assumed that the points were sufficiently close together such that an approximately linear trend can be seen between them. Within this interpolation scheme, energy was represented by the x variables, and cross section was represented by the y variables. The interpolation assumed that all energy values and cross sections were known on the endpoints of a given interval, and that the unknown value was the cross section at the midpoint. Interpolation was performed at 0.05 eV increments. Outside of the relevant energy ranges, cross sections were assumed to be zero. For example, in Yoon's article, in Table 5 on page 921 vibrational cross sections were presented only between 0.55 eV and 100 eV. Therefore, at energies above 100 eV and below 0.55 eV, the cross section was taken to be zero. As a further example, in Table 11 on page 925, dissociation cross sections were shown only between 9 eV and 80 eV. Below 9 eV and

above 80 eV, then, the dissociation cross sections were taken to be zero. In Itikawa's article, in Table 4 vibrational cross sections for O_2 were given only between 5 and 15 eV. So, at energies outside of these two limits, the vibrational data for O_2 were taken to be zero. Similar arguments can be made for oxygen dissociation and ionization cross sections. The final detail for the database is that cross sections in each source were presented for only limited ranges of electron energies. Outside of the limits provided, cross sections were taken to be zero simply due to the absence of data. Once the interpolation was performed, the function placed all original and interpolated points for hydrogen and oxygen cross sections in tables. These tables are included as an appendix.

3.2.3. Chemical Kinetics. Rate coefficients and cross sections can be used to determine the changes in concentrations of reactants and products. In general, assuming reactions with multiple steps, the net rate of production for a given species will be the difference between reaction rates that produce the required species minus the reaction rates that destroy that species. More explicitly, this concept can be shown in Eq. 26.

$$net\ rate\ of\ production = creation\ rate - destruction\ rate \tag{26}$$

For single step mechanisms, creation rates in Eq. 26 can be described by the forward rate coefficients from Eq. 18 and concentrations of reactants. Concentrations of electrons are represented by the third body concentrations *[M]* in Eqs. 27-29. Recombination rates are represented by k_{rc}, and dissociation rates are represented by k_d. Molecular concentrations are represented by $[A_2]$. Equation 27 represents the creation rate for dissociated atoms in a unimolecular reaction at low pressures.

$$\frac{d[A]}{dt} = k_d[A_2][M] - k_{rc}[A][M] \tag{27}$$

The total rate of dissociation is equal to the rate of reaction which creates dissociated atoms minus the rate of destruction of dissociated atoms. This rate of destruction in Eq. 27 is equal to the rate at which dissociated atoms recombine. Creation rates of excited molecules can be described by Eq. 28.

$$\frac{d[A_2^*]}{dt} = k_e[A_2][M] - (k_d[A_2^*][M] + k_i[A_2^*][M]) \quad (28)$$

Here the rates of destruction are equivalent to sum of the dissociation and ionization rates, since both of these reactions "destroy" an excited molecule. Dissociation rate coefficients are denoted by k_d, excitation rate coefficients are represented by k_e, and ionization rate coefficients are represented by k_i. Similarly, the creation rate for ionization is shown in Eq. 29, where the rate of destruction is represented by the dissociation and electron absorption rates.

$$\frac{d[A_2^+]}{dt} = k_i[A_2][M] - \left(k_d[A_2^+][M] + k_a[A_2^+][M]\right) \quad (29)$$

Rates of destruction were neglected since, kinetically, data on the reverse reactions were unavailable. A future, more accurate and robust analysis must include these terms. Chemical rate equations can be used to determine how the concentrations of products vary with time. Over a given time interval these rates, in general, are given by Eqs. 30-32. Initially, at time t = 0 s, the concentrations, inlet temperature, and pressure are assumed to be known values.

$$Excitation: \quad [A_2^*]_t = [A_2^*]_{t-1} + k_e[A_2]_{t-1}[e^-]t \quad (30)$$

$$Dissociation: \quad [A]_t = [A]_{t-1} + k_d[A_2]_{t-1}[e^-]t \quad (31)$$

$$Ionization: \quad [A_2^+]_t = [A_2^+]_{t-1} + k_i[A_2]_{t-1}[e^-]t \quad (32)$$

In the above equations, t represents a given time in seconds, and concentrations (terms in brackets) at each new time are calculated on a molar basis. At each iteration the new concentration available (t-1 term) is constantly updated with the concentration of the previous time step. It is also important to note that at each time step, the concentration of reactant molecules available will change and must be updated. This rate of loss of

reactant molecules is equivalent to the sum of the excitation, dissociation, and ionization creation rates in Eq. 27-29.

3.2.4. Energy Loss Analysis. Energy loss of the electron traveling through gas can also be modeled to assess the overall penetration depth of the beam and the number and type of collisions that can be expected. This problem examines the number and type of collisions a well as the penetration depth of an electron as it travels in one-dimensional motion through molecular hydrogen (H_2) or molecular oxygen (O_2) gas contained in a cylinder. The electron energy changes with collisions in the gas. For this problem, the electron is tested at a starting energy of 998 eV for both gases since cross sections were only provided up to a maximum of 998 eV for oxygen. This aspect allows tests for each gas to have equivalent, reliable starting energies for comparison of corresponding results. The basic geometry for penetration depth is shown in Figure 3.5.

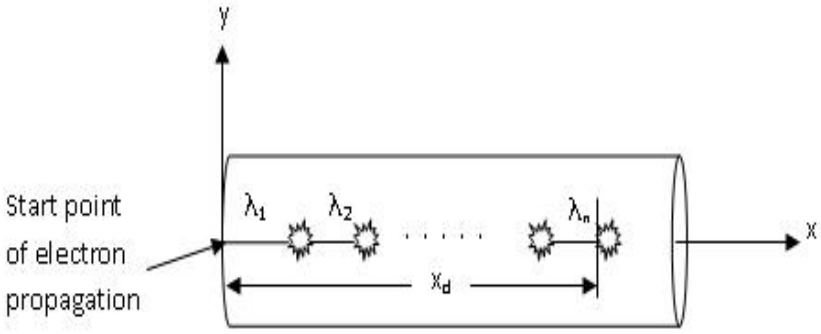

Figure 3.5. Penetration depth geometry

In Figure 3.5, the cylinder containing hydrogen or oxygen is arbitrarily oriented in the x-axis. The symbol λ_1, λ_2, and λ_n are mean free paths of varying size that are dependent upon the gas number density and cross section. The star symbols represent electron collisions with molecules. The variable x_d represents the total penetration depth of an electron at a specific energy. The cylinder is assumed to be completely filled with gas up to its boundaries. Walls of the cylinder are assumed to simply confine the gas to a volume, and their thickness is neglected. Electron scattering and absorption effects are

ignored for this approximation. Recombination after dissociation is also ignored. The electron emanates from a point source located at the origin (0,0,0) and travels down the tube in only the positive x direction. The electron is assumed to move by an amount equivalent to the mean free path (mfp) before and otherwise between collisions. Mean free path is defined as the distance that the electron travels between collisions. For this initial approximation, the mfp is calculated according to Eq. 33.

$$\lambda = \frac{1}{n\sigma} \tag{33}$$

In Eq. 33, n represents the number density of the hydrogen gas in particles per cubic meter. The symbol σ represents the cross section (m^2) at the specified energy in electron-volts (eV). Equation 33 does not account for the mean, relative speed of the molecules since E_{el} is much greater than the thermal energy of the gas. In other words, the hydrogen gas is essentially stationary in relation to the high speed motion of the electrons [13]. Number density can be described a function of the pressure, temperature, and Boltzmann constant, as in Eq. 34.

$$n = \frac{p}{kT} \tag{34}$$

As the electron travels through the gas it will have collisions with various molecules in the gas. At each collision the electron will lose a given amount of energy to the molecule it strikes. For this model, the electron is assumed to excite, dissociate, or ionize the molecule. Elastic collisions are not considered. What type of collision occurs and how much energy is lost is governed by the dominant (i.e. largest) cross section at a given electron energy and the excitation, dissociation, or ionization potential. The first ionization potential (FIP) is defined as the amount of energy required to cause ionization in either an atomic element or molecule. The dissociation potential is defined as the amount of energy required to cause dissociation, and the excitation potential is defined as the amount of energy required to cause excitation. Molecular hydrogen has a FIP of approximately 15.4 eV [14]. It has a dissociation potential of approximately 4.5 eV [15]

and an excitation potential of approximately 0.516 eV [11]. Oxygen has a FIP of 12.0697 eV, a dissociation potential of 5.12 eV, and an excitation potential of 0.196 eV. Values of excitation potential and dissociation potential for oxygen are obtained from JANNAF Thermochemical Tables NSRDS-NBS 37 Table 7.1 [16]. Ionization potential for oxygen is obtained from the National Institute of Standards and Technology (NIST) Chemical Kinetics Database [17]. For a given type of collision, the assumption is made that the electron loses an amount of energy equivalent to the values just stated. The appropriate potential is chosen by examining the largest cross section at a given energy in the database. For example, if, at a given electron energy of 500 eV, the largest cross section was for hydrogen dissociation, then the electron loses 4.5 eV to the hydrogen molecule, and dissociation occurs. Dissociation reactions continue to occur with the electron losing 4.5 eV each time until the largest cross section at a given energy changed to a different mode (excitation or ionization). Similar arguments are made for the cases involving excitation or ionization. Equation 35 provides the basic relationship used to determine the energy loss of the electron, where EP is the excitation potential, DP is the dissociation potential, and FIP is the first ionization potential. The potential that is used depends on the reaction that occurs during a given collision.

$$E_{new} = E_{old} - EP, DP, or\ FIP \tag{35}$$

Each iteration starts with an E_{new} that was calculated by subtracting the ionization, dissociation, or excitation potential from the previous iteration's electron impact energy. The process continues until the electron energy is zero. At each point during calculations, electron energy, excitation cross sections, dissociation cross sections, ionization cross sections, the amount of energy lost, mean free path, collision time, penetration depth, number density, and dominant cross section are stored in a table. After the data is compiled in the table, the number of a given type of collision can be determined by simply examining the energy lost at each collision and performing a summation for each group of collisions showing the same energy lost. Total penetration depth x_d can be calculated by taking the summation of all mean free paths, since λ is the average distance traveled between collisions.

A disadvantage of this kinetic approach is that it assumes that there is always a collision between the electron and a molecule. It further assumes that the collision will cause a reaction corresponding to only a single mode. In reality, a collision can cause any of the three aforementioned modes, none of them, or some combination of the three. There can also be recombination of products after reaction or absorption of free or beam electrons after ionization. Additionally, depending on aspects such as number density, scattering, and whether or not the electron and molecule have a finite relative velocity, a collision is not always guaranteed to occur [13]. Collisions that result in a given reaction require more energy than just a simple, random collision. Rates of the reaction will also be less than the overall collision rate [13]. Finally, when calculating changes in concentrations of various products, degradation of energy for electrons in the beam must be determined. As a beam travels through the gas the electrons in it collide with and lose energy to the molecules. Over a long spatial distance or time interval, a beam which enters at a given energy (such as 1000 eV) will degrade to some lesser energy value further downstream. This will affect the size of the rate coefficient ($f\sigma v$) since the impact cross section and electron velocity are energy dependent. As the electron energy changes within the beam, so will the size of the rate coefficient. Rate coefficients, then, would not be inherently constant. So, during each iterative step, concentrations would be more accurately calculated by allowing for this change in Eqs. 27-32. Rate coefficients would be accounted for by combining the energy loss mechanism and the chemical kinetics described in this section through statistical means such as a Monte Carlo technique.

4. ANALYSIS OF RESULTS

4.1. THERMAL MODEL RESULTS

Mole fractions of dissociated hydrogen and oxygen are 0.5 for the thermal model at approximate levels of energy addition of $1.3x10^{8}$ kJ/kg for H and $9.2x10^{6}$ kJ/kg for O. Correspondingly, molar concentrations for these energy amounts are $1.7x10^{-3}$ mol/m^3 for H and $1.6x10^{-3}$ mol/m^3 for O. Thermal mole fractions for H_2 and O_2 are compared in Figure 4.1a and Figure 4.1b. The point where 50% dissociated H or O is produced is around 3350 K for hydrogen and 3420 K for oxygen.

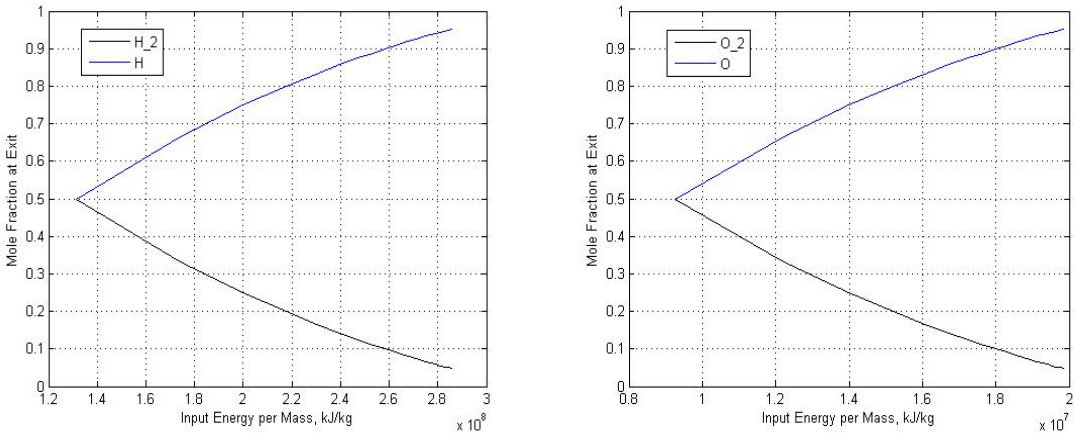

(a) (b)

Figure 4.1. Mole fractions for thermal dissociation (a) Mole fractions for thermal dissociation of H_2 (b) Mole fractions for thermal dissociation of O_2

Note that the plots start at the point where more H or O begins to be produced. These plots would continue to the left at lower energy values. At energy values below the minimums shown, more molecules and fewer dissociated atoms would be present in the mixture. Creation of a mixture containing 90 percent H or O requires $2.6x10^{8}$ kJ/kg and $1.8x10^{7}$ kJ/kg of thermal energy, respectively. The lighter H_2 gas requires an amount of energy that is an order-of-magnitude higher than the heavier O_2 gas. This fact relates to the strength of the bonds between the atoms and the energy required to break them.

Heats-of-formation for hydrogen at the specified exit states are larger than those for oxygen at the same states, indicating a larger amount of energy is necessary to break the chemical bonds and cause dissociation. For stated exit ratios, equilibrium constants are a maximum of 0.5 for a 1:1 ratio for both hydrogen and oxygen. In Figure 4.2a and Figure 4.2b, exit temperatures for various exit ratios are compared for hydrogen and oxygen dissociation, respectively.

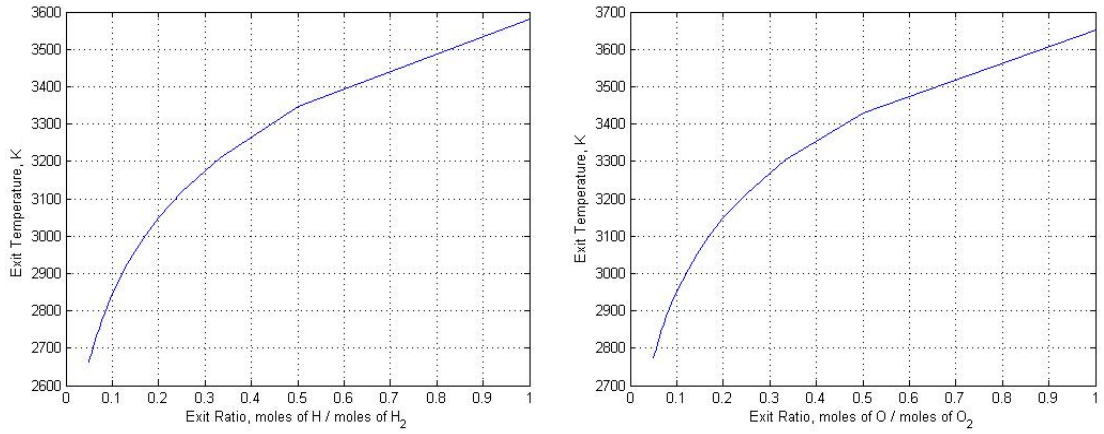

(a) (b)

Figure 4.2. Exit temperatures for thermal dissociation (a) H_2 (b) O_2

As the mole fraction of a given product increases as a result of more energy input, the equilibrium constant will also increase in size. As exit ratios and required energy increase, the exit temperatures increase. For exit ratios between 1:20 and 1:1, the thermal exit temperature range is 2666 K - 3581 K for hydrogen and 2775 K - 3651 K for oxygen. A ratio of 2:1 provides an exit temperature of approximately 3823 K for hydrogen and 3875 K for oxygen. The amount of heat available to inject into the gas will generally be dependent on material considerations in the heater and gas cylinder, as well as the capacity of the heater itself. The large energy requirements for thermal dissociation are a result of the simultaneous application of the energy to all components of the gas.

4.2. KINETIC MODEL RESULTS

Results for this model indicate qualitatively that kinetic modification of a gas is possible. The amount of excitation, dissociation, or ionization is related to the electron energy, cross sections, and the amount of time the beam is applied to the gas. The following sections describe the effectiveness of the electron impact on molecules in a volume of gas.

4.2.1. Rate Coefficients. Results for the kinetic model show that, for electron energies between 0 - 1000 eV, rates of forward reaction for excitation, dissociation, and ionization are between $0.1x10^{-7}$ - $2x10^{-7}$ cm^3/s and $0.1x10^{-8}$ - $3.5x10^{-8}$ cm^3/s respectively, for the mono-energetic and Maxwellian energy distributions. Forward reaction rates are shown Figure 4.3a for the Maxwellian distribution and in Figure 4.3b for the mono-energetic electron beam.

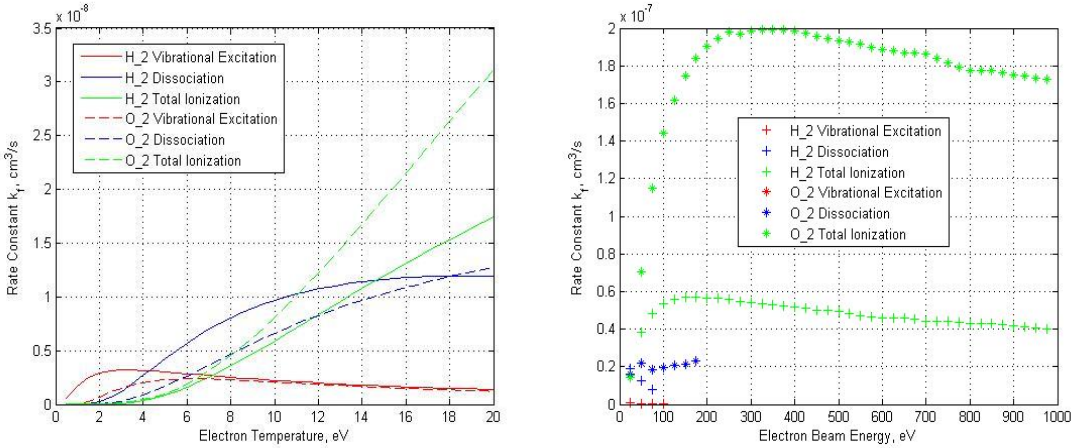

(a) (b)

Figure 4.3. Rate coefficients for H_2 and O_2 (a) Maxwellian rate coefficients (b) mono-energetic rate coefficients

Examining Figure 4.3a and Figure 4.3b, the rate coefficients show that pure kinetic reactions do not occur with any significant speed for either energy distribution. Qualitatively, there are specific ranges where a given mode of kinetic reaction is dominant. For example, in the Maxwellian distribution, hydrogen dissociation rates are

dominant between electron temperatures of 5 eV and 11 eV. Oxygen ionization rates are dominant above 12 eV. Excitation rates for hydrogen are largest for electron temperatures between 0 eV to 4 eV. Oxygen excitation and dissociation rates are dominant in the same regions as hydrogen but these rates are much smaller than their hydrogen counterparts. Figure 4.3b shows that the oxygen ionization rates are much higher than any other rates presented for beam energies greater than approximately 50 eV. Below 50 eV, dissociation effects are generally dominant for both hydrogen and oxygen. It must also be noted that the dissociation and ionization effects are generally larger for the mono-energetic beam. As an example, at 50 eV the dissociation rate coefficients for oxygen and hydrogen are approximately $0.2\text{x}10^{-7}$ cm^3/s and $0.17\text{x}10^{-7}$ cm^3/s. This translates more obviously to values of $2\text{x}10^{-8}$ cm^3/s for oxygen and $1.7\text{x}10^{-8}$ cm^3/s, clearly larger than even the largest Maxwellian dissociation rate (H_2) of $1\text{x}10^{-8}$ cm^3/s. A similar effect is also noticed for the ionization rate coefficients provided beam energies are greater than 50 eV ($0.7\text{x}10^{-7}$ cm^3/s and $0.39\text{x}10^{-7}$ cm^3/s, respectively). Below this energy, the rate coefficients are smaller (~$1\text{x}10^{-8}$ cm^3/s) than those produced by the Maxwellian distribution provided the Maxwellian electron temperature is kept above 11 eV. An electron temperature under 11 eV provides rate coefficients on the order of $1\text{x}10^{-9}$ cm^3/s to $7.5\text{x}10^{-9}$ cm^3/s. The mono-energetic beam will provide faster rates of dissociation and ionization provided that the beam energy is above 50 eV. The Maxwellian distribution will provide faster rates of excitation. Note that mono-energetic excitation rates are essentially zero while the Maxwellian distribution provides excitation rates between $0.1\text{x}10^{-8}$ cm^3/s and $0.4\text{x}10^{-8}$ cm^3/s. These rates of reaction demonstrate the possibility that the kinetic beams can be tuned to specific reactions. In Figure 4.3a and 4.3b, certain rates are dominant in certain ranges of energy. Setting the beam to a specific energy will cause faster rates of reaction for certain modes as compared to other modes thereby increasing the probability of higher concentrations of a specific type.

4.2.2. Concentrations. Slow rates of forward reaction are further exhibited in product concentrations shown in Figures 4.4 – 4.8. In each plot, molar concentrations are graphed as a function of time. Concentrations were presented for a beam containing $6.242\text{x}10^{18}$ electrons. Larger concentrations of dissociated and ionized molecules are

produced by the mono-energetic beam. Maximum mono-energetic hydrogen excitation occurs for a 25 eV beam with $2.3x10^{-19}$ mol/cm^3 at 40 seconds.

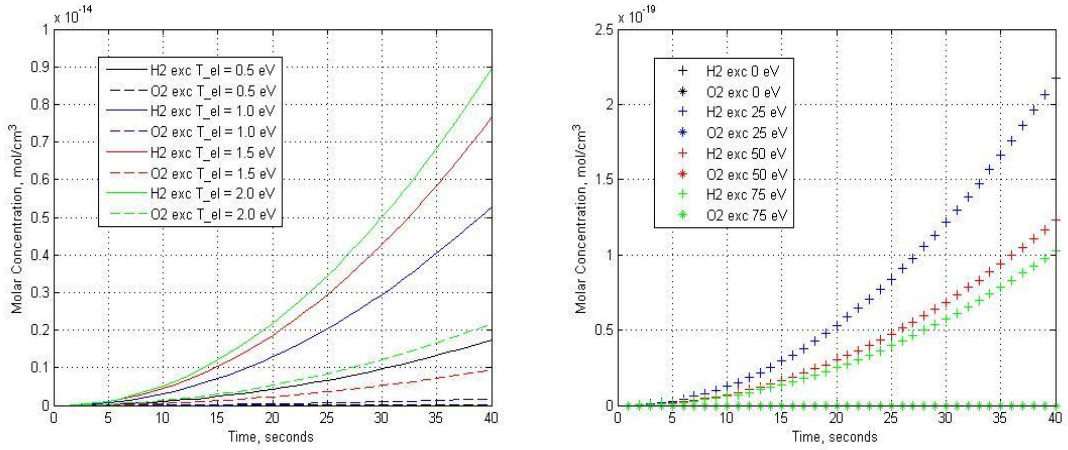

(a) (b)

Figure 4.4. Molar concentrations of excited molecules (a) Maxwellian distribution (b) mono-energetic distribution

According to Figure 4.4a, molar concentrations of excited hydrogen for the Maxwellian distribution are largest at an electron temperature of 2 eV where the concentration is $0.9x10^{-14}$ mol/cm^3 at 40 seconds. In this case, excited oxygen concentrations are largest for the 2 eV beam where the concentration is $0.2x10^{-14}$ mol/cm^3 at 40 seconds. Molar concentrations of excited oxygen show no significant increase for beam energies less than 75 eV for the mono-energetic distribution shown in Figure 4.4b. Examining Figure 4.4b further shows that excitation concentrations are larger for a 25 eV beam than the 75 eV beam. Electron energy dependent cross sections are a dominant factor in the size of reaction rates and concentrations of products. The reason for this is due to the size of the cross sections at those energies. Recalling Figure 3.3, the excitation cross sections are largest at low energies (around 25 eV). Cross sections at 75 eV are smaller than those at 25 eV. These cross sections are major factors in the calculation of the rate coefficients and corresponding chemical kinetics used to obtain concentrations (see section 3.2.3). Smaller cross sections lead to lower reaction rates and lower concentrations. An

analogous argument can be made for the Maxwellian distribution plots for excitation. This fact is also seen in the concentration plots for dissociation and ionization for either distribution.

Dissociated concentrations are shown in Figure 4.5a and Figure 4.5b. Maxwellian concentrations are $8x10^{-16}$ mol/cm^3 for hydrogen dissociation and $1x10^{-16}$ mol/cm^3 for oxygen dissociation at 40 seconds. Hydrogen has larger dissociation rates due its larger dissociation cross sections. Dissociation and ionization concentrations are higher for the mono-energetic beam. In the range shown in Figure 4.5b, dissociated hydrogen concentrations are largest at 25 eV where the concentration is $6x10^{-14}$ mol/cm^3 at 40 seconds. This beam energy is within the range where cross sections and corresponding rate coefficients are dominant for hydrogen dissociation. Dissociated oxygen concentrations are largest at 50 eV ($7x10^{-14}$ mol/cm^3 at 40 s), but are much larger due to the larger cross sections and rate coefficients present at that energy. Comparing the hydrogen and oxygen data, the concentration at 40 seconds is larger for hydrogen dissociation whereas the concentration at 40 seconds for ionization is larger for oxygen.

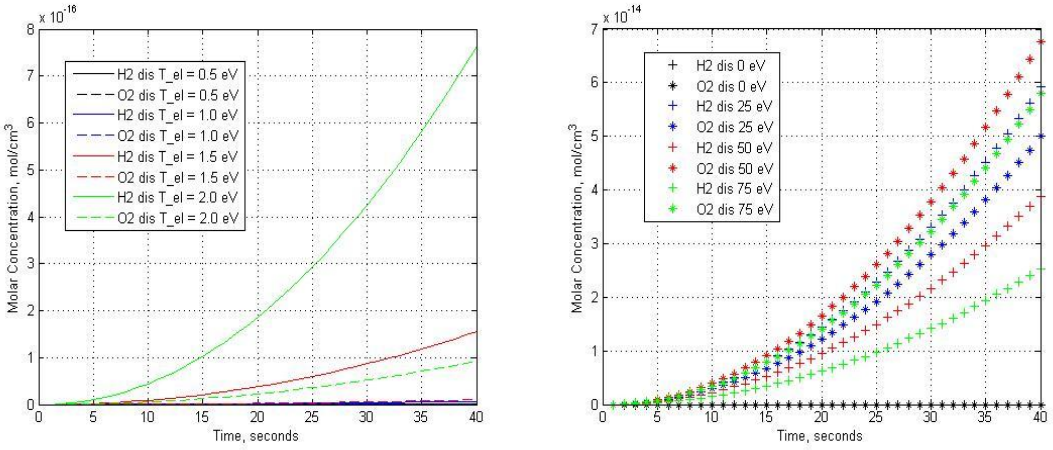

(a) (b)

Figure 4.5. Molar concentrations of dissociated molecules (a) Maxwellian distribution (b) mono-energetic distribution

Ionized concentrations are shown in Figure 4.6a and Figure 4.6b. Note for the mono-energetic case in Figure 4.6b, the ionization concentrations at 25 eV are nearly identical in magnitude over the 40 second time interval (see Figure 4.6b blue markers). Approximately equivalent magnitudes for each data set are due to the nearly identical cross section size and rate coefficients for hydrogen and oxygen at this energy. Maximum molar concentrations shown in Figure 4.6b for H_2 and O_2 with the mono-energetic beam are approximately $3.5x10^{-17}$ mol/cm^3 at 75 eV for O_2 ions, and $1.5x10^{-17}$ mol/cm^3 at 75 eV for H_2 ions. Reaction rates for ionization begin to decrease above 100 eV and will result in decreasing concentrations of ions produced. Maximum molar concentration at an electron temperature of 2 eV for the Maxwellian distribution is approximately $2.7x10^{-17}$ mol/cm^3 for oxygen ionization at 40 seconds. Maximum molar concentration at an electron temperature of 2 eV for the Maxwellian distribution is $1.5x10^{-17}$ mol/cm^3 for hydrogen ionization respectively over a 40 second time interval.

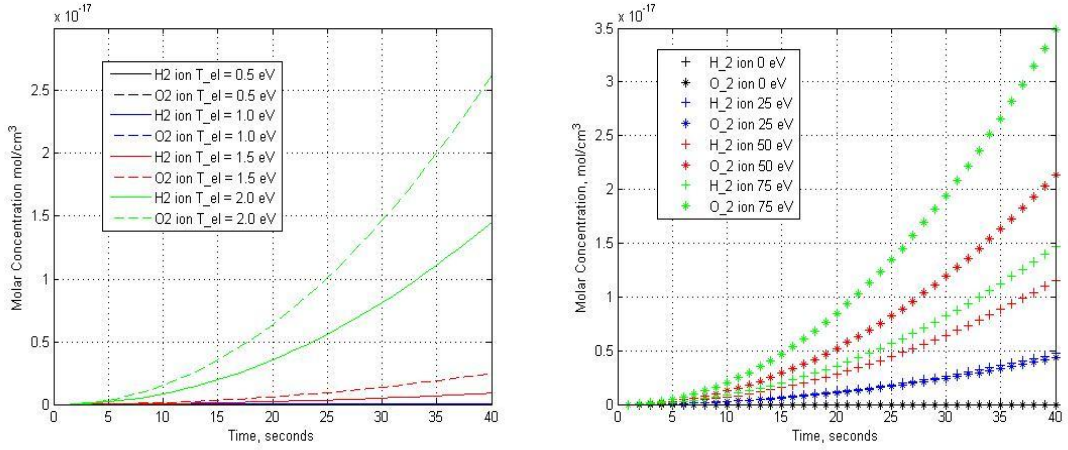

(a) (b)

Figure 4.6. Molar concentrations of ionized molecules (a) Maxwellian distribution (b) mono-energetic distribution

4.2.3. Penetration Depth. Penetration depths in Figure 4.7 and Figure 4.8 were compiled for four different pressures and temperatures for both hydrogen and oxygen. Each circle in the plots represents a single collision event. Once an excitation,

ionization, or dissociation event occurs, the changed molecule or atom is removed from consideration in the system. The penetration depth x_d was a measure of the total distance traveled by the electron at a specific energy. In both cases, the largest penetrations occur for the highest temperatures and lowest pressures. Lower pressures will naturally have a lower density and will therefore allow electrons to move more freely through a given volume. Temperature affects the distance since the number density is a function of this quantity as well as pressure. The number density in a gas can therefore decrease for an increase in temperature with pressure held constant. It will increase for higher pressure with temperature held constant. In turn, a larger number density will decrease the mean free path (see Eq. 34). A smaller number density will increase the mean free path. At 450 K and 1 atm, hydrogen gas allows the largest propagation distance at 1.47 mm. At the same temperature and pressure, oxygen has a propagation distance of approximately 1.3 mm. In each of the four cases, the electron travels a slightly smaller distance in oxygen as compared to hydrogen. In test case 2, maximum penetration for the electron in hydrogen is approximately 0.5 mm while the penetration into oxygen is approximately 0.5 mm. An increase in temperature to 450 K while holding pressure constant (test case 4) causes an increase in penetration of approximately 0.25 mm for hydrogen and an increase of 0.23 mm for oxygen penetration. For hydrogen in each case there are 64 ionization collisions, 1 dissociation collision, and 15 excitation collisions. Oxygen energy loss analysis shows 81 ionization collisions, 1 dissociation collision, and 40 excitation collisions for each test case. Figure 4.7 and Figure 4.8 show that the oxygen ionization collisions occur within a much shorter spatial distance than the hydrogen ionization collisions. This is due to the difference in ionization potential and the cross sections for ionization for each gas. Beam electrons in oxygen lose 12.1 eV per ionization while beam electrons in hydrogen lose 15.4 eV per ionization. This fact means that larger ionization cross sections remain in detection and allow smaller mean free paths to occur (inverse proportionality). Therefore, the ionization collisions occur over a shorter distance in oxygen. Beam electrons lose energy faster to ionization in hydrogen due to the larger ionization potential which means the mean free path decreases more rapidly and fewer collisions can occur. An analogous situation can be noted for the

excitation collisions since the excitation potential is approximately 0.2 eV in oxygen as opposed to approximately 0.5 eV in hydrogen.

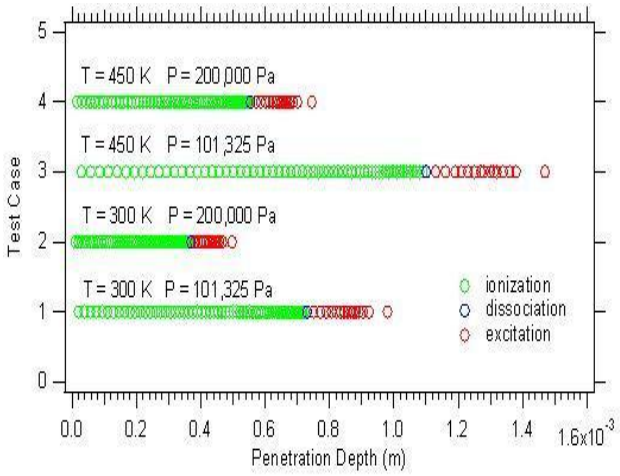

Figure 4.7. Penetration depth of electron into H_2

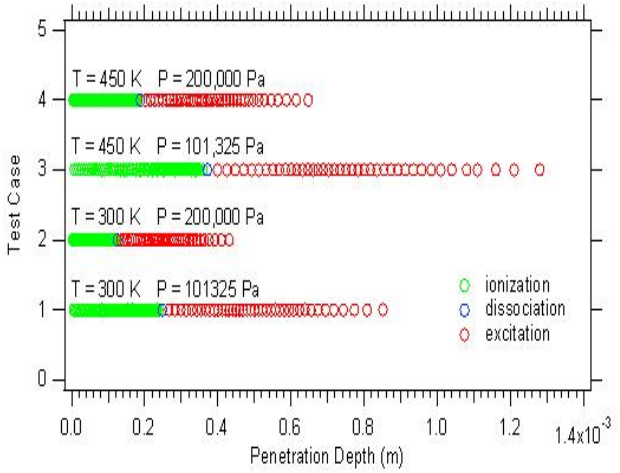

Figure 4.8. Penetration depth of electron into O_2

In reality, these propagation distances are dependent on more than just mean free path and number density. Penetration depth also depends on scattering angles of the electron, beam electrons lost due to absorption, and if the electron loses more (or less)

energy than just the assigned potential for a given type of collision. Steric factors for given types of collision also affect penetration depths. Steric factors relate to the molecules or atoms having a high probability for the correct orientation to cause a specific reaction. For example as a thought experiment, in dissociation, a molecule oriented perpendicularly to the direction of the impacting electron will have a higher probability of dissociation as opposed to a molecule oriented in a parallel manner with respect to the impacting electron. This result is due to the electron impacting the molecule directly on the bond in the former case rather than impacting on an end molecule present in the molecular chain.

4.2.4. Error Sources. In the energy loss model, each collision caused the electron to lose a prescribed amount of energy depending on the type of collision. As an example, for hydrogen ionization the electron lost 15.4 eV. Oxygen ionization caused the electron to lose 12.1 eV. Since the electron loses less energy per collision in the oxygen case the electron will be able to cause more collisions of a given type as it moves through the gas. Limitations are that the electron will lose at least its ionization, dissociation, or excitation potential for a given reaction. The model presented here assumes that the molecule has sufficient energy and the preferred orientation to allow a reaction. However, it may also lose more energy for a given reactive collision. It may also lose less energy than is required for a reaction. Future energy loss modeling must account for these effects to properly assess the penetration depth. As the electron loses greater amounts of energy, collisions occur initially with greater and then less frequency. This is due to the size of the collision cross section at a given electron energy. Recalling Figure 3.3, as the electron energy increases the size of the cross section initially increases and then decreases with higher energies. Since mean free path is inversely proportional to the cross section, it will decrease with the increase in cross section at a specified energy up to a specified point. Then it will begin to increase with the decrease in the size of the cross section. As the electron gains more energy, the kinetic energy and velocity of the electron will increase. At lower energy ranges, the electron velocity and molecular velocity will be more comparable in size and the cross section may increase. This will introduce a $\sqrt{2}$ into the mean free path calculation. Larger velocity means the electron will move through a given spatial distance in a shorter time, thereby decreasing the

probability that the relative motion of a molecule will be quick enough to cross the path of the electron and cause a reactive collision. This aspect will also cause the mean free path to increase in size. In Figure 4.7 test-case 3 (TC3), hydrogen ionization collisions between 0.5 mm and 0.7 mm show large spacing, between 0.7 mm and 1.1 mm the spacing between collisions is drastically reduced. Further, in Figure 4.8 TC3, excitation collisions between 0.35 mm and 0.5 mm have larger spacing, then as the dominant excitation cross section initially increases, the spatial distance decreases and collision frequency increases between 0.5 mm and 0.9 mm. Beyond 0.9 mm, as the cross section decreases, the mean free path increases and the corresponding collision frequency decreases. Differences in the number of collisions and their corresponding type shown in Figure 4.7 and Figure 4.8 can be further explained by the mechanism of operation for the energy loss code. First, inspecting Figure 3.3, cross section data exists over only specific energy ranges. Limited range for cross section data institutes error into the results when determining the dominant cross sections for mean free path calculations. If no data exists at a given energy (i.e. equals 0), then the code must compare the data points remaining, if any, that are not zero. Otherwise the code must choose the one cross section that does exist at that energy. So, depending on the energy, an accurate determination of the dominant cross section may not be made. Inaccurate determination of the dominant cross section leads to an incorrect amount of energy being subtracted from the electron (a wrong collision type determined). An incorrect loss of energy contributes to a different number of distances and corresponding collision types being used in calculations. Different numbers of collision points resulting from a given starting energy demonstrates that different amounts of energy subtracted will lead to slower or faster rates of energy degradation thereby increasing or decreasing the mfp. Larger or smaller mfp distances calculated between collisions will affect the total distance traveled as well as the number and types of collisions shown. Additionally, in Figure 4.7 and Figure 4.8, there are more or less collisions of a given type due to how much energy is lost. As an example, hydrogen loses 15.4 eV per ionization collision, 4.5 eV per dissociation collision, and 0.5 eV per excitation collision. Oxygen loses 12.1 eV per ionization collision, 5 eV per dissociation collision, and 0.2 eV per excitation collision. Put simply, an electron losing more energy per collision will take less time and distance to reach its termination point (0

eV) than an electron losing less energy. Greater energy loss also means many more cross sections (possibly dominant ones) will be skipped over during the searches conducted for calculation of mean free path and energy loss. This results in fewer collisions and reactions than if less energy is lost per collision.

Finally, there is also uncertainty contained in the calculations for kinetic rate coefficients and kinetic concentrations. This uncertainty arises from the percent errors for the cross section data provided in Section 3.2.2. Recall that cross sections were explicitly used to calculate rate coefficients and concentrations. They were also the governing factor on how much energy was lost by an electron for a given type of collision. These percent errors in cross sections (see Section 3.2.2) will propagate through the aforementioned calculations. Rate coefficients, kinetic concentrations, and the penetration analysis will then contain noticeable amounts of uncertainty that will be greater than, or at least equal to, the original cross section error used for the given calculation. Reaction rate coefficient and concentration uncertainty will likely be greater than ±20 percent for hydrogen excitation, hydrogen dissociation, and oxygen excitation. Error for oxygen dissociation will be a value larger than ±34 percent. Uncertainty for hydrogen ionization will likely be greater than ±7 percent, and oxygen ionization uncertainty should be greater than ±5 percent.

4.3. COMPARISON OF MODELS

A direct comparison of the thermal and kinetic data is limited. Data show that the thermal model provides the most significant change in the gas, but it requires energy on the order of $10^{7} – 10^{8}$ J/kg to produce the changes. Thermal mole fractions between 50-90% H or O can be obtained if enough energy is added to the system. The amount of thermal energy that can be added will be limited by power and material constraints. Kinetic data show for the energy range tested between 0-1000 eV that there is no significant change in the gas. Recall that kinetic concentrations for both distributions were on the order of $10^{-7} – 10^{-11}$ mol/cm^{3}. This is *not* demonstrating that thermal energy addition is better than kinetic energy addition. It does reveal that the modeling techniques used provide inconclusive results for comparison. Recall that thermal energy range required for significant hydrogen dissociation was between $1.4x10^{8} – 2.6x10^{8}$ J/kg

(50-90% H). The range for thermal dissociation of oxygen was between $1x10^{7}$ – $1.8x10^{7}$ J/kg (50-90% O). Maximum concentrations of thermally produced H and O are $2.5x10^{-3}$ mol/cm^3 at $2.7x10^{8}$ J/kg and $2.5x10^{-3}$ mol/cm^3 at $1.9x10^{7}$ J/kg. In contrast, the maximum electron beam energy range tested was between 0 eV and 1000 eV. Converting this value to Joules produces a range between extremely small values of only 0 J - $1.602x10^{-16}$ J per electron resulting in approximately 999.9 J of energy being injected for $6.242x10^{18}$ electrons in the beam. Concentrations for kinetic excitation, dissociation, and ionization were then between orders-of-magnitude of 10^{-19} – 10^{-14} mol/cm^3. Values of this size result in mole fractions that are zero. There is no real change in the gas for the energy range tested in the kinetic model. From a qualitative perspective, the kinetic model shows that the beam needs to be active for at least 20 seconds to begin showing large amounts of growth in any of the three modes. This is likely due to the small reaction rates seen in Figure 4.5 and Figure 4.6 that are used to calculate the concentrations. The small amount of kinetically deposited energy is the direct contributor to the small, kinetically produced concentrations seen in Figures 4.4-4.8. Energies of the kinetic beam must be larger in order to quantify the baseline beam energy at which a noticeable change in either gas begins to occur. Furthermore, energies above 1000 eV, including energies equivalent to those seen in the thermal model, must be tested to be able to quantify the benefits of kinetically modifying a gas as opposed to thermal modification. Simulations with higher electron energies will also demonstrate that kinetic modification can produce equivalent or better product concentrations for less energy than required by the thermal case. Penetration depths can be better simulated by incorporating statistical methods to model electron trajectories and wall losses. Statistical methods may also better quantify the actual amount of energy lost to various types of collisions.

5. CONCLUSIONS AND FUTURE RESEARCH

Based on stated results, kinetic mole fractions show no significant change from the inlet, reactant species for the energy range tested between 0 – 1000 eV. Thermal energy deposition provides a more pronounced change in the gas but for very large energy requirements (10^7-10^8 kJ/kg). A better comparison of the methods would be provided by using kinetic beam energies on the same order-of-magnitude as those presented in the thermal model. This would require the associated cross sections for these conditions, which were unavailable for this project. Therefore, the benefits of the kinetic beam over the thermal energy deposition cannot be quantified using the modeling techniques presented in this research. What is revealed, at least qualitatively, is that the kinetic beam shows that it can have a high level of selectivity toward specific reactions according to cross sections and reaction rates. Kinetic beam selectivity indicates that less energy than thermal deposition would be expended to obtain the same amount of or more reactions in the gas. Since reaction potentials for the individual reactions are just a few electron-volts, targeting and causing a specific reaction should indeed require less energy than thermal deposition which targets numerous reactions simultaneously. Unfortunately, the modeling techniques employed in this research were unable to reveal the extent of this energy difference. More complex, three dimensional modeling incorporating statistical analysis (Monte Carlo technique) and a more extensive cross section database must be used in future research to quantitatively describe the kinetic interactions and benefits. Error in the cross section measurements and subsequent calculations should also be monitored to minimize uncertainty present in the results and provide a more reliable and robust analysis of the data. Experiments could also be used to quantitatively compare the results of each mode of energy deposition, but would not be as useful in understanding the fundamental nature of the interactions since only the final results of the processes would be observed.

Within the kinetic model, qualitative examination reveals that the mono-energetic beam produces larger concentrations of dissociated atoms and ionized molecules for beam energies above 50 eV. Kinetic modification using the Maxwellian distribution produces larger concentrations of excited hydrogen or oxygen molecules. As stated, each

energy distribution shows some ability to be tuned in such a way as to cause a specific mode of reaction to occur. The mono-energetic beam is the most feasible for tuning effects since all electrons are at a single energy and can be targeted to cause a single reaction. However, recalling Figure 3.3, cross sections of some finite size exist at all energies in the tested range; some cross sections are just significantly larger than others in a given range (i.e. ionization). Ability to tune the beam energy, then, is limited to a given beam having only a higher probability of a given reaction taking place kinetically. These same facts are true for the Maxwellian distribution. Tuning the beam energy is more difficult, though, since the Maxwellian distribution has groups of electrons at different energies in a single given beam. Dominant reactions at a specific electron temperature occur for all three modes simultaneously. Speeds of reaction partly depend on the actual number of electrons at a specific energy. Since the Maxwellian distribution qualitatively provides faster excitation rates and the mono-energetic beam has faster dissociation and ionization rates, it may be best for future models or experiments to employ a beam source capable of producing both distributions. It first generates a Maxwellian distribution to more quickly excite atoms and molecules in the mixture. Faster excitation rates more quickly produce molecules at the appropriate energies to readily dissociate or ionize. At this point, then, the source produces the mono-energetic beam to provide faster dissociation or ionization, depending on which type of free radical is most desired.

Future kinetic analysis must be conducted using higher energy electrons (>1000 eV) and their associated cross sections to improve performance of the kinetic model. Higher energy electrons will allow larger penetration depths so that a larger volume of gas can be affected. Higher energies will also create faster forward reaction rates and higher corresponding concentrations of products. These beam energies must also be on the same order-of-magnitude as the thermal energy addition to provide a better, direct comparison between the two modeling techniques. Greater kinetic beam energies will quantitatively demonstrate that a kinetic beam provides more significant changes for less energy expenditure when compared with the thermal energy addition. Analysis must also include calculation of electron impact cross sections by using the appropriate integrals. Empirical cross section tables and plots are limited to the energy range, gas temperature, and gas pressure that were tested to produce them. These integral calculations will allow

the determination of cross sections at any temperature, pressure, and electron energy, and will allow quantification of the effects of the kinetic beam interaction with hydrogen or oxygen gas. Once these improvements are incorporated, a more complete description of the processes within the gas can be developed to provide more detailed insight into the benefits of kinetic modification.

APPENDIX

MATLAB CODES ON CD-ROM

BIBLIOGRAPHY

[1] Starikovskaia, S.M., "Plasma assisted ignition and combustion," Journal of Physics D: Applied Physics, Vol. 39, 2006, R265-R299.

[2] Ombrello, Timothy, Xiao Qin, Yiguang Jin, Alexander, Fridman, Alexander, "Enhancement of Combustion and Flame Stabilization Using Stabilized Non-Equilibrium Plasma," *43th AIAA Aerospace Sciences Meeting and Exhibit*, 2005-1194, AIAA, Princeton University, Princeton, New Jersey 08544, Drexel University, Philadelphia, Pennsylvania 19104, 10-13 Jan. 2005.C. L. Seitz, "System Timing," in *Introduction to VLSI Systems*, Addison-Wesley, pp. 218-262, 1980.

[3] Ombrello, Timothy, Xiao Qin, Yiguang Jin, Shailesh Gangoli, Gutsol, Alexander, Fridman, Alexander, "Non-equilibrium Plasma Discharge: Characterization and Effect on Ignition," *44th AIAA Aerospace Sciences Meeting and Exhibit*, 2006-1214, AIAA, Department of Mechanical and Aerospace Engineering, Princeton University, Princeton, New Jersey 08544, Drexel Plasma Institute, Mechanical Engineering and Mechanics Department, Drexel University, Philadelphia, Pennsylvania 19104, 9-12 Jan. 2006.

[4] Macheret, Sergey O., Shneider, Mikhail N., Miles, Richard B., "Electron Beam Generated Plasmas in Hypersonic MHD Channels," Princeton University, Department of Mechanical and Aerospace Engineering, D-414 Engineering Quadrangle, Princeton, New Jersey 08544-5263, *American Institute of Aeronautics and Astronautics*, 1999.

[5] Penetrante, B.M., Hsiao, M.C., Bardsley J.N., Merritt B.T., Vogtlin, G.E., Wallman, P.H., Kuthi, A., Burkhart, C.P., Bayless, J.R., "Electron Beam and Pulsed Corona Processing of Volatile Organic Compounds and Nitrogen Oxides", Lawrence Livermore National Laboratory, Livermore, California 94550 USA. First Point Scientific, Inc. Agoura Hills, California 91301 USA, Figure 3.

[6] JANNAF Thermochemical Tables, Thermal Research Laboratory, The Dow Chemical Company, Midland, Michigan.

[7] Cengel, Yunus A. and Boles, Michael A., *Thermodynamics: An Engineering Approach. Fourth Edition*, , McGraw-Hill Higher Education, The McGraw-Hill Companies, Inc., 1221 Avenue of the Americas, New York, New York 10020, 2002, Chap. 14.

[8] Turns, Stephen R., *An Introduction to Combustion: Concepts and Applications*, 2nd ed., McGraw-Hill Higher Education, A Division of The McGraw-Hill Companies, 2006, pp. 626-629, pp. 642-645.

[9] Levine, Raphael D., *Molecular Reaction Dynamics*, Press Syndicate of the University of Cambridge. Cambridge University Press. The Edinburgh Building, Cambridge, CB2 2RU, United Kingdom, 40 West 20th Street, New York, New York 10011-4211, 2005, pp. 75, 79.

[10] Chen, Francis F., *Introduction to Plasma Physics and Controlled Fusion Volume 1: Plasma Physics* 2nd ed., Springer Science+Business Media, LLC, 2006, 233 Spring Street, New York, NY, 10013, pp. 225-229.

[11] J. Yoon, M. Song, J. Han, S. Hwang, W. Chang, B. Lee, and Y. Itikawa,"Cross Sections for Electron Collisions with Hydrogen Molecules," *Journal of Physical and Chemical Reference Data,* Vol. 37, No. 2, 2008, pp. 918-926.

[12] Itikawa, Y., "Cross Sections for Electron Collisions with Oxygen Molecules," *Journal of Physical and Chemical Reference Data,* Vol. 38, No. 1, 2009, pp. 8, 13-14.

[13] Vincenti, Walter G. and Kruger, Charles H. Jr., *Introduction to Physical Gas Dynamics*, Krieger Publishing Company, Malabar, Florida, 1965, pp. 14 & 215.

[14] Herzberg, G., *Physical Review Letters,* Vol. 23, No. 19, 1969, Division of Pure Physics, National Research Council of Canada, Ottawa, Canada, pp. 1081-1083.

[15] Gaydon, A.G., *Dissociation Energies and Spectra of Diatomic Molecules*, Dover Publications, Inc. 1950, p. 209.

[16] JANNAF Thermochemical Tables, *NSRDS-NBS 37*, Table 7.1.

[17] National Institute of Standards Chemical Kinetics Database, NIST URL:http://webbook.nist.gov/cgi/cbook.cgi?ID=C7782447&Units=SI&Mask=20#Ion-Energetics [cited 15 Oct. 2010].

VITA

John Benjamin Gaither was born on April 10, 1983 in Little Rock, Arkansas. He spent his childhood in Benton, Arkansas where he graduated from high school in May 2001. John was accepted to the University of Missouri-Rolla during the fall of the same year. From 2007 to 2009, he was involved in a design team to create and test a microgravity welding apparatus at NASA Ellington Field as part of the Reduced Gravity Flight Opportunities Program. He twice assisted with the simulated microgravity testing of the experiment as a flyer onboard the aircraft as both an undergraduate and graduate student. He was also active as a member of the university's symphonic band as an undergraduate. He has also worked as an engineering intern for the Materials Division of the Arkansas Highway and Transportation Department during the summer and winter breaks of 2006 and 2007. While there, he assisted in implementing SiteManager database software which tracked and managed all highway materials projects in the state of Arkansas. In May 2008, he received his Bachelor of Science Degree in Aerospace Engineering from the Missouri University of Science and Technology.

John currently lives in Rolla, Missouri where he attends the Missouri University of Science and Technology as a graduate student. Between 2008 and 2010, he worked as a graduate teaching assistant for two core curriculum, aerospace laboratory classes. He will be earning his Master's of Science Degree in Aerospace Engineering in May 2011.